

Double perovskite oxides $\text{La}_2\text{NiMnO}_6$ and $\text{La}_2\text{Ni}_{0.8}\text{Fe}_{0.2}\text{MnO}_6$ for inorganic perovskite solar cells

Sergey S. Kozlov¹, Olga V. Alexeeva¹, Anna B. Nikolskaia¹, Oleg I. Shevaleevskiy^{1,a}, Denis D. Averkiev², Polina V. Kozhuhovskaya^{2,3}, Oksana V. Almjasheva^{2,3,b}, Liudmila L. Larina¹

¹Solar Photovoltaic Laboratory, Emanuel Institute of Biochemical Physics, Moscow, Russia

²St. Petersburg State Electrotechnical University “LETI”, St. Petersburg, Russia

³Ioffe Physical-Technical Institute, St. Petersburg, Russia

^ashevale2006@yahoo.com, ^balmjasheva@mail.ru

Corresponding author: Anna B. Nikolskaia, anickolskaya@mail.ru

PACS 84.60.Jt

ABSTRACT Nanopowders of $\text{La}_2\text{Ni}_{0.8}\text{Fe}_{0.2}\text{MnO}_6$ and $\text{La}_2\text{NiMnO}_6$ double perovskite oxides were synthesized by glycine-nitrate combustion method. The obtained materials were characterized using X-ray diffraction, scanning electron microscopy and optical measurements. Thin nanostructured layers based on the prepared materials were used as light absorbing layers for fabrication of inorganic perovskite solar cells (PSCs). Electron transport layers for the PSCs were prepared using TiO_2 and ZrO_2 nanostructured layers. The best performance of 3.7 % under AM1.5G illumination was obtained for the PSC structure glass/FTO/ $\text{ZrO}_2/\text{La}_2\text{Ni}_{0.8}\text{Fe}_{0.2}\text{MnO}_6/\text{Spiro-MeOTAD}/\text{Au}$.

KEYWORDS nanostructures, double perovskite oxides, perovskite solar cells, solar photovoltaics

ACKNOWLEDGEMENTS This work was supported by the Russian Science Foundation under grant No. 20-69-47124.

FOR CITATION Kozlov S.S., Alexeeva O.V., Nikolskaia A.B., Shevaleevskiy O.I., Averkiev D.D., Kozhuhovskaya P.V., Almjasheva O.V., Larina L.L. Double perovskite oxides $\text{La}_2\text{NiMnO}_6$ and $\text{La}_2\text{Ni}_{0.8}\text{Fe}_{0.2}\text{MnO}_6$ for inorganic perovskite solar cells. *Nanosystems: Phys. Chem. Math.*, 2022, **13** (3), 314–319.

1. Introduction

Nanostructured materials are widely used for the development of next-generation *solar cells* since they allow one to fabricate *high efficiency* and low-cost devices which are promising for mass production *photovoltaic technologies* [1, 2]. In the last decade, numerous studies in the area of solar photovoltaics were focused on the development of perovskite solar cells (PSCs) [3]. In PSCs an organic-inorganic hybrid material with perovskite-like structure ABX_3 ($\text{A} - \text{CH}_3\text{NH}_3^+$, $\text{HC}(\text{NH}_2)_2^+$, $\text{B} - \text{Pb}^{2+}$, Sn^{2+} , $\text{X} - \text{I}^-$, Br^- , Cl^-) is used as a light absorbing layer which is deposited on the surface of a nanostructured electron transport layer (ETL) [3–5]. Over a short period of time the power conversion efficiency (PCE) of lab-scale PSCs was increased from 3 – 5 % to 20 – 25 % that is comparable to the performance of conventional crystalline silicon solar cells [6, 7]. Low production costs make PSCs the most promising candidates for the future photovoltaic technologies. At the same time, conventional perovskite materials are not stable and degrade under high humidity conditions, light irradiation and increased temperatures [8, 9]. Yet another issue is the presence of the toxic lead cation Pb^{2+} in the B-site position of conventional hybrid perovskites [10, 11]. Therefore, the search for the new environmentally friendly and stable perovskite materials with the improved parameters is an essential task of the modern photovoltaics.

Recently it was reported that the $\text{A}_2\text{B}'\text{B}''\text{O}_6$ type double perovskite oxides (A is alkaline earth or rare-earth species and B'/B'' are 3d transition species) can be used as a light absorbing photoactive material in PSCs [12, 13]. Such inorganic compounds as $\text{Ln}_2\text{NiMnO}_6$, where $\text{Ln} = \text{La}$, Eu , Dy or Lu , are characterized by a narrow energy band gap, long carrier lifetime, and good stability under high temperatures and humidity levels [14, 15]. The first attempts to fabricate $\text{Ln}_2\text{NiMnO}_6$ -based PSCs resulted in poor photovoltaic parameters where the efficiency was less than 1 % [14]. To improve the performance, cation doping was used that caused the increase of the transport characteristics of double perovskite oxides [16, 17]. A significant increase of the PCE was reached with the introduction of metal atom in the B' -site position that improved the electronic properties of $\text{La}_2\text{NiMnO}_6$ material by increasing the concentration of charge carriers [18].

In this work, nanoparticles of $\text{La}_2\text{Ni}_{1-x}\text{Fe}_x\text{MnO}_6$ ($x = 0, 0.2$) double perovskite oxides were synthesized by glycine-nitrate combustion method and their structures were investigated using X-ray diffraction (XRD), X-ray fluorescence analysis (XRF), energy dispersive X-ray microanalysis (EDXMA) and scanning electron microscopy (SEM). Using the

obtained materials for the preparation of the light absorbing layers, we fabricated a series of PSC samples with the following architectures: (1) glass/FTO/ TiO_2 / $\text{La}_2\text{NiMnO}_6$ /Spiro-MeOTAD/Au, (2) glass/FTO/ TiO_2 / $\text{La}_2\text{Ni}_{0.8}\text{Fe}_{0.2}\text{MnO}_6$ /Spiro-MeOTAD/Au, (3) glass/FTO/ ZrO_2 / $\text{La}_2\text{NiMnO}_6$ /Spiro-MeOTAD/Au, (4) glass/FTO/ ZrO_2 / $\text{La}_2\text{Ni}_{0.8}\text{Fe}_{0.2}\text{MnO}_6$ /Spiro-MeOTAD/Au and investigated their photovoltaic characteristics.

2. Experiment

2.1. Materials and samples preparation

The $\text{La}_2\text{NiMnO}_6$ (LMNO) and $\text{La}_2\text{Ni}_{0.8}\text{Fe}_{0.2}\text{MnO}_6$ (LMNO(Fe)) double perovskite oxide nanopowders were synthesized by glycine nitrate combustion method ($G/N = 0.55$) using corresponding salts according to the procedure described in [19]. The obtained materials were mixed with acetic acid, terpineol, ethyl cellulose and ethanol to obtain homogeneous pastes as specified in [20]. The pastes were sonicated in ultrasonic bath several times and deposited by screen-printing onto FTO conductive glass substrates (Solaronix, 2×2 cm) with subsequent annealing at 500°C for 1 hour to form thin layers for SEM and optical measurements. LMNO and LMNO(Fe)-based homogeneous pastes were then used as precursors for spin coating perovskite light absorbing layers in the process of PSC device fabrication [21].

2.2. Device fabrication

Schematic representation of the PSC architecture is illustrated in Fig. 1. The electron transport layers (ETLs) were fabricated using TiO_2 and ZrO_2 materials. For this purpose, we used commercially available TiO_2 nanoparticles (Degussa-P25) and ZrO_2 nanoparticles prepared by dehydration of co-precipitated hydroxides under hydrothermal conditions. The method was described in our previous work [22]. Nanostructured TiO_2 and ZrO_2 ETLs with 200 nm thickness were deposited on conductive FTO (fluorine-doped tin oxide) glass substrates using spin-coating method at 2000 rpm for 1 min, followed by sintering at 500°C for 30 min. Next, the light absorbing active layer based on inorganic double perovskite oxide LMNO or LMNO(Fe) and a hole transport layer (HTL) based on Spiro-MeOTAD (Sigma-Aldrich) were successively deposited on the ETL surface. Fabrication of the PSCs was completed by the deposition of Au electrodes with a thickness of 50 nm using thermal evaporation. As a result, we fabricated 4 series of the PSC samples with the following architectures: (1) glass/FTO/ TiO_2 / $\text{La}_2\text{NiMnO}_6$ /Spiro-MeOTAD/Au, (2) glass/FTO/ TiO_2 / $\text{La}_2\text{Ni}_{0.8}\text{Fe}_{0.2}\text{MnO}_6$ /Spiro-MeOTAD/Au, (3) glass/FTO/ ZrO_2 / $\text{La}_2\text{NiMnO}_6$ /Spiro-MeOTAD/Au, and (4) glass/FTO/ ZrO_2 / $\text{La}_2\text{Ni}_{0.8}\text{Fe}_{0.2}\text{MnO}_6$ /Spiro-MeOTAD/Au.

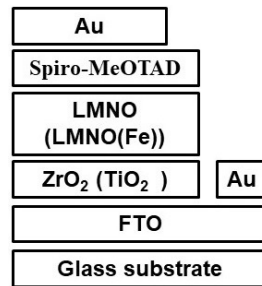


FIG. 1. Schematic representation of the PSC architecture

3. Characterization studies

XRD measurements of LMNO and LMNO(Fe) nanoparticles were provided using DRON-3M X-ray diffractometer with $\text{CuK}\alpha$ radiation ($\lambda = 1.5405 \text{ \AA}$) as the X-ray source. The elemental composition of the powders was determined by XRF on a Spectroscan GF-2 X-ray fluorescence spectrometer and EDXMA using Vega 3 Tescan scanning electron microscope with the EDAX energy dispersive analyzer. SEM images of the specially prepared perovskite layers on glass substrates were obtained by Hitachi SU8000 field-emission scanning electron microscope (FE-SEM). The optoelectronic properties of the perovskite layers were characterized using UV-Vis spectrophotometer (Shimadzu UV-3600, Japan) with an ISR-3100 integrating sphere in the wavelength range of 300 – 1400 nm.

Photovoltaic (PV) characteristics of the developed PSCs were measured under standard illumination conditions (AM1.5G , 1000 W/m^2) by recording the current-voltage (I - V) characteristics using Keithley 4200-SCS Semiconductor Characterization System (Keithley, USA) and Abet Technologies 10500 solar simulator with Xenon lamp (Abet, USA) as the light source. The PCE (η) values of the PSCs was calculated from the I - V data using the known formula:

$$\eta = \frac{J_{SC} \cdot V_{OC} \cdot FF}{P_{IN}} \cdot 100 \%, \quad (1)$$

where J_{SC} is the short-circuit current density, V_{OC} is the open-circuit voltage, FF is the fill factor and P_{IN} is the incoming light intensity.

4. Results and discussion

XRD patterns of the LMNO and LMNO(Fe) nanopowders are shown in Fig. 2. The peaks indicate the single-phase perovskite structure and the purity of all samples. The reflexes are recorded for monoclinic, rhombohedral and orthorhombic structures confirming the triple phase structure of double perovskite oxides such as $\text{La}_2\text{NiMnO}_6$ [23]. Table 1 shows the chemical composition and the crystallite size of the synthesized LMNO and LMNO(Fe) nanopowders determined by EDXMA and XRF measurements.

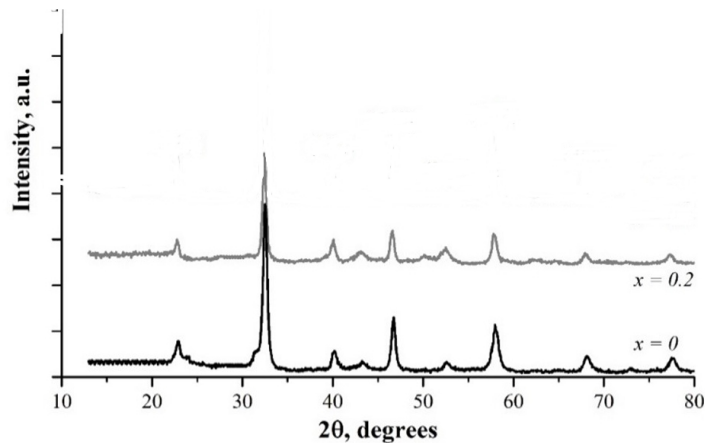


FIG. 2. XRD patterns of $\text{La}_2\text{NiMnO}_6$ and $\text{La}_2\text{Ni}_{0.8}\text{Fe}_{0.2}\text{MnO}_6$ nanopowders

TABLE 1. Chemical composition and average crystallite size for powders of the double perovskite oxides prepared

Sample	Method	Chemical composition, mol. %				Average crystallite size, nm
		La	Ni	Fe	Mn	
$\text{La}_2\text{NiFeMnO}_6$	EDXMA	52.5	25.6	0.0	21.9	18 ± 1
$\text{La}_2\text{Ni}_{0.8}\text{Fe}_{0.2}\text{MnO}_6$	EDXMA	46.7	25.4	6.6	21.3	20 ± 1
	XRF	50.9	22.2	5.7	21.2	

SEM images of thin LMNO and LMNO(Fe) layers deposited on glass substrates show porous structure of the layer surfaces (see Fig. 3). It could be seen that LMNO sample exhibits large amount of macropores, while in LMNO(Fe) their number is significantly lower. Besides that, LMNO(Fe) sample possesses more uniform surface and denser morphology which is important for light energy absorbing layer in high efficient PSCs. The decrease in pore size and the enhancement of uniformity of the LMNO(Fe) thin layer in comparison with LMNO sample can be attributed to the partial B'/B'' cation ordering in the crystal structure initiated by the introduction of Fe^{3+} ions. It is known that $\text{La}_2\text{NiMnO}_6$ is characterized by a disordered structure in which Ni^{2+} , Ni^{3+} , Mn^{3+} , Mn^{4+} cations randomly occupy B-positions whereas the introduction of Fe^{3+} ions lead to a predominant content of Ni^{2+} and Mn^{4+} ions and to their stricter placement in the lattice structure [24].

The optical measurements have shown that the band gaps for the fabricated thin perovskite layers, calculated from the Tauc plots [25], were 1.18 and 1.28 eV for LMNO and LMNO(Fe), respectively (see Fig. 4). The band gap of the synthesized LMNO(Fe) is close to the Shockley-Queisser limit of 1.34 eV, which provides the maximum power conversion efficiency for the single-junction solar cell [26]. Thus, due to the lower band gap, synthesized LMNO(Fe) double perovskite oxide can absorb larger part of solar radiation in comparison with the halide perovskite $\text{CH}_3\text{NH}_3\text{PbI}_3$ with a band gap of 1.5 – 1.6 eV, which is used in conventional PSCs [27].

Table 2 summarizes the details on the architectures of the fabricated PSCs and the PV parameters obtained. Inorganic PSCs based on both undoped and Fe^{3+} doped LNMO layers with TiO_2 ETLs exhibited *poor PV characteristics* (see Table 2). To improve the performance of LNMO-based PSCs, we used the ETLs based on very wide band-gap ZrO_2 nanostructured layers with the band gap of ~ 6 eV, which was much larger than that for the TiO_2 layer (3.2 eV). Previously we have shown that the charge transport mechanisms at the perovskite/ETL interfaces was entirely different in ZrO_2 ETL in comparison with TiO_2 ETL [22].

Figure 5 presents schematic energy band diagrams for the developed PSCs based on double perovskite LNMO(Fe) light absorbing layers with TiO_2 and ZrO_2 ETLs. It could be seen that developed PSCs have different interface electronic

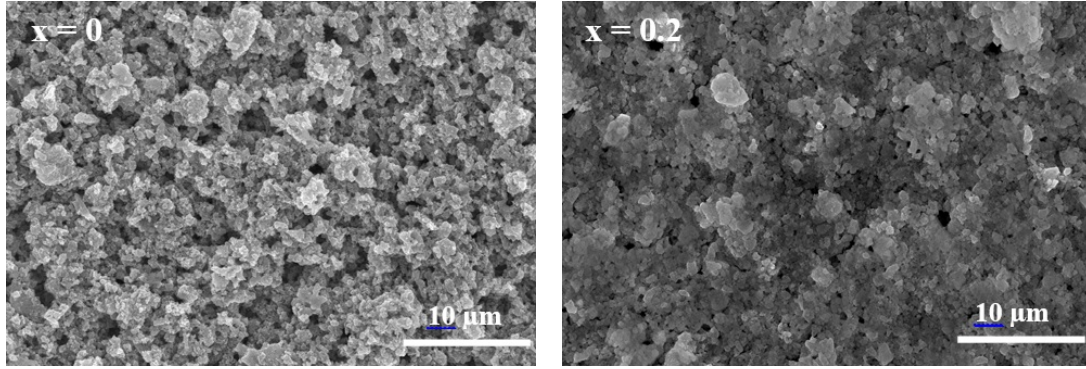


FIG. 3. SEM surface images of LMNO (left) and LMNO(Fe) (right) thin layers

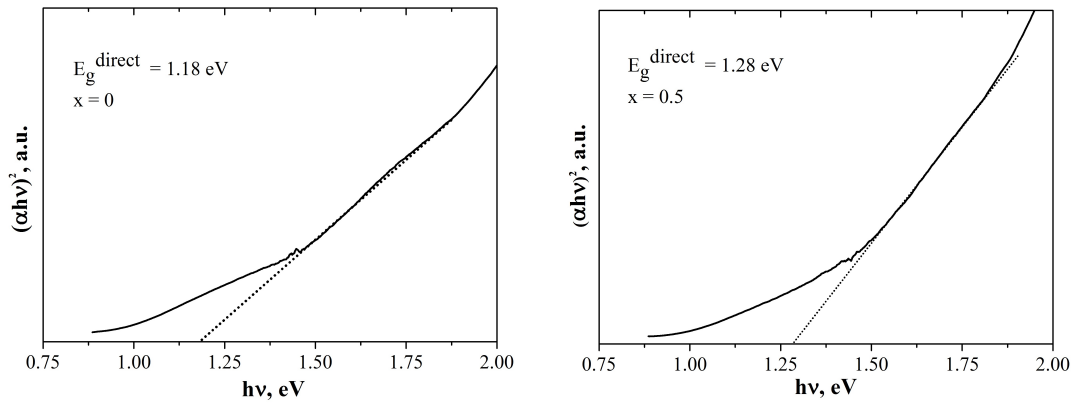


FIG. 4. Tauc plots of LMNO (left) and LMNO(Fe) (right) thin layers

TABLE 2. The architectures of inorganic PSCs and their photovoltaic characteristics under simulated AM 1.5G irradiance

	ETL	Perovskite light absorbing layer	HTL	J_{SC} , mA/cm^2	V_{OC} , mV	FF , a.u.	η , %
1	TiO_2	$\text{La}_2\text{NiMnO}_6$	Spiro-MeOTAD	1.2	470	0.4	0.22
2	TiO_2	$\text{La}_2\text{Ni}_{0.8}\text{Fe}_{0.2}\text{MnO}_6$	Spiro-MeOTAD	1.6	495	0.47	0.37
3	ZrO_2	$\text{La}_2\text{NiMnO}_6$	Spiro-MeOTAD	6.5	700	0.49	2.2
4	ZrO_2	$\text{La}_2\text{Ni}_{0.8}\text{Fe}_{0.2}\text{MnO}_6$	Spiro-MeOTAD	8.5	740	0.58	3.7

structures, although both interfaces show the spike conduction band offsets. At the $\text{TiO}_2/\text{LNMO}(\text{Fe})$ interface (Fig. 5a), the conduction band (CB) of the LMNO(Fe) perovskite is located 0.4 eV below the CB of the TiO_2 ETL. Such band energy structure reduces the efficient charge transfer across the perovskite/ETL interface to the front FTO electrode and leads to the significant decrease of the device performance. However, valence bands (VBs) structure at the LMNO(Fe)/Spiro-MeOTAD interface found to be favorable for the efficient hole transfer providing the pathways to the Au back electrode. The obtained PV parameters and the PCEs of the developed PSCs with TiO_2 ETLs were poor (see Table 2). A slight improvement of the PV parameters was observed for LMNO(Fe)-based PSCs in comparison with LMNO ones, which could be attributed to the higher light absorption ability due the larger E_g value of LMNO(Fe) perovskite material and better morphology of LMNO(Fe) ETL layer.

Incomparably higher conduction band offset is realized at the perovskite/ETL interface when using ZrO_2 ETLs (Fig. 5b). Indeed, the CB of the LMNO(Fe) perovskite absorbing layer is located 1.6 eV below the CB position of ZrO_2 ETL. Such energy band offset blocks the charge transfer across the perovskite/ETL interface. So, the alternative conductivity mechanism could be considered. In our previous publications, we reported on the successful application of the ZrO_2 ETL in the fabrication of inorganic PSCs based on the BiFeO_3 perovskite light absorbing layers [22]. It was shown that charge transfer across the $\text{BiFeO}_3/\text{ZrO}_2$ interface was quite efficient regardless the unfavorable interface electronic structure, in which the CB of the BiFeO_3 perovskite layer was located 1.1 eV below the CB of the ZrO_2 ETL.

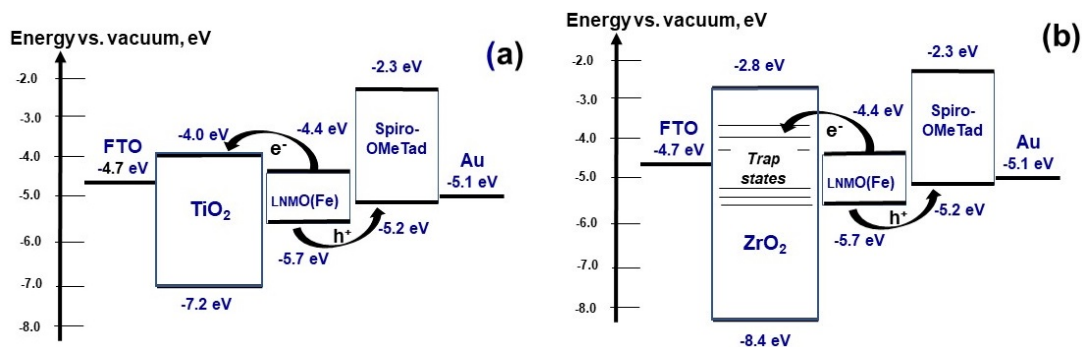


FIG. 5. Schematic energy band diagrams for the PSCs based on double perovskite LMNO(Fe) light absorption layers with ZrO_2 (a) and TiO_2 (b) ETLs

The observed effective electron transfer across perovskite/ ZrO_2 interface could be described to the hopping conduction through the localized states within the forbidden zone of ZrO_2 due to the large concentration of the nanoparticle surface defects [20]. Several publications confirmed that nanostructured layers based on very wide band gap ($E_g > 5$ eV) materials with negligible density of the electrons in the CB provide the effective transfer due to the large concentration of the surface defects in the forbidden zone. Thus, we have found that the best PCE value of 3.7 % was observed for the PCS device with glass/FTO/ ZrO_2 / $\text{La}_2\text{Ni}_{0.8}\text{Fe}_{0.2}\text{MnO}_6$ /Spiro-MeOTAD/Au architecture. The new approach for fabrication all inorganic PSCs based on double perovskite oxides with record photovoltaic parameters was developed.

5. Conclusions

Nanopowders of double perovskite oxides $\text{La}_2\text{NiMnO}_6$ and $\text{La}_2\text{Ni}_{0.8}\text{Fe}_{0.2}\text{MnO}_6$ were synthesized using glycine-nitrate combustion method and used to fabricate thin nanostructured light absorbing layers for the inorganic PSCs. XRD, SEM and optical measurements of the prepared layers revealed that the introduction of Fe^{3+} ions into the crystal structure of $\text{La}_2\text{NiMnO}_6$ material improves the structural properties of the perovskite layer and increases in the optical band gap value from 1.2 to 1.3 eV. For the first time the PSCs based on the LNMO and LNMO(Fe) double perovskite oxides with ZrO_2 -based ETLs were developed, and their photovoltaic properties were studied. Thus, we have fabricated the series of the PSCs with the following architectures: (1) glass/FTO/ TiO_2 / $\text{La}_2\text{NiMnO}_6$ /Spiro-MeOTAD/Au, (2) glass/FTO/ TiO_2 / $\text{La}_2\text{Ni}_{0.8}\text{Fe}_{0.2}\text{MnO}_6$ /Spiro-MeOTAD/Au, (3) glass/FTO/ TiO_2 / $\text{La}_2\text{NiMnO}_6$ /Spiro-MeOTAD/Au, (4) glass/FTO/ ZrO_2 / $\text{La}_2\text{Ni}_{0.8}\text{Fe}_{0.2}\text{MnO}_6$ /Spiro-MeOTAD/Au. The best performance was obtained for the LNMO(Fe)-based PSC with ZrO_2 ETL, showing PCE value of 3.7 % under AM1.5G illumination conditions. This value was significantly higher as compared to the PCE values observed for PSCs based on the TiO_2 ETLs. It was also shown that very wide-bandgap ETLs provide efficient electron transfer described by hopping transport mechanism.

References

- [1] Shubbak M.H. Advances in solar photovoltaics: Technology review and patent trends. *Renew. Sustain. Energ. Rev.*, 2019, **115**, 109383.
- [2] Green M. Photovoltaic technology and visions for the future. *Progr. Energ.*, 2019, **1** (1), 013001.
- [3] Lu H., Krishna A., et al. Compositional and interface engineering of organic-inorganic lead halide perovskite solar cells. *iScience*, 2020, **23** (8), 101359.
- [4] Tejeda A., Choy W.C.H., Deleporte E., Graetzel M. Hybrid perovskites for photovoltaics and optoelectronics. *J. Phys. D: Appl. Phys.*, 2020, **53** (7), 070201
- [5] Ansari M.I.H., Qurashi A., Nazeeruddin M.K. Frontiers, opportunities, and challenges in perovskite solar cells: a critical review. *J. Photochem. Photobiol. C: Photochem. Rev.*, 2018, **35**, P. 1–24.
- [6] Green M.A., Dunlop E.D., et al. Solar cell efficiency tables (version 58). *Prog. Photovolt.: Res. Appl.*, 2021, **29**, P. 657–667.
- [7] Park N.G. Research direction toward scalable, stable, and high efficiency perovskite solar cells. *Adv. Energy Mater.*, 2020, **10** (13), 1903106.
- [8] Bisquert J., Juarez-Perez E.J. The causes of degradation of perovskite solar cells. *J. Phys. Chem. Lett.*, 2019, **10** (19), P. 5889–5891.
- [9] Wang H.-Q., Wang S., et al. Understanding degradation mechanisms of perovskite solar cells due to electrochemical metallization effect. *Sol. Energ. Mater. Sol. Cell.*, 2021, **230**, 111278.
- [10] Schileo G., Grancini G. Lead or no lead? Availability, toxicity, sustainability and environmental impact of lead-free perovskite solar cells. *J. Mater. Chem. C*, 2021, **9**, P. 67–76.
- [11] Su P., Liu Y., et al. Pb-based perovskite solar cells and the underlying pollution behind clean energy: dynamic leaching of toxic substances from discarded perovskite solar cells. *J. Phys. Chem. Lett.*, 2020, **11**, P. 2812–2817.
- [12] Yin W.-J., Weng B., et al. Oxide perovskites, double perovskites and derivatives for electrocatalysis, photocatalysis, and photovoltaics. *Energy Environ. Sci.*, 2019, **12**, P. 442–462.
- [13] Lan C., Zhao S., et al. Investigation on structures, band gaps, and electronic structures of lead free $\text{La}_2\text{NiMnO}_6$ double perovskite materials for potential application of solar cell. *J. Alloy. Comp.*, 2016, **655**, P. 208–214.
- [14] Sheikh M.S., Ghosh D., et al. Lead free double perovskite oxides $\text{Ln}_2\text{NiMnO}_6$ (Ln = La, Eu, Dy, Lu), a new promising material for photovoltaic application. *Mater. Sci. Eng. B*, 2017, **226**, P. 10–17.

- [15] Kumar M., Raj A., Kumar A., Anshul A. Theoretical evidence of high power conversion efficiency in double perovskite solar cell device. *Opt. Mater.*, 2021, **111**, 110565.
- [16] Xu X., Zhong Y., Shao Z. Double perovskites in catalysis, electrocatalysis, and photo(electro)catalysis. *Trends Chem.*, 2019, **1** (4), P. 410–424.
- [17] Afroze S., Karim A.H., et al. Latest development of double perovskite electrode materials for solid oxide fuel cells: a review. *Front. Energ.*, 2019, **13** (4), P. 770–797.
- [18] Shi J., Gan H., Wang C., Shen Q. Fe-doping effect on magnetic properties of $\text{La}_2\text{CoMnO}_6$ ceramics prepared by plasma activated sintering. *J. Eur. Ceram. Soc.*, 2021, **41**, P. 6516–6522.
- [19] Popkov V.I., Almjashaeva O.V., et al. Magnetic properties of YFeO_3 nanocrystals obtained by different soft-chemical methods. *J. Mater. Sci. Mater. Electron.*, 2017, **28**, P. 7163–7170.
- [20] Ito S., Chen P., et al. Fabrication of screen-printing pastes from TiO_2 powders for dye-sensitized solar cells. *Prog. Photovolt.: Res. Appl.*, 2007, **15**, P. 603–612.
- [21] Nikolskaia A.B., Kozlov S.S., et al. Cation doping of $\text{La}_2\text{NiMnO}_6$ complex oxide with the double perovskite structure for photovoltaic applications. *Russ. J. Inorg. Chem.*, 2022, **67** (6), P. 921–925.
- [22] Vildanova M.F., Nikolskaia A.B., Kozlov S.S., Shevaleevskiy O.I. Charge transfer mechanisms in multistructured photoelectrodes for perovskite solar cells. *J. Phys. Conf.*, 2020, **1697** (1), 012187.
- [23] Sheikh M.S., Sakhya A.P., Dutta A., Sinha T.P. Light induced charge transport in $\text{La}_2\text{NiMnO}_6$ based Schottky diode. *J. Alloy. Comp.*, 2017, **727**, P. 238–245.
- [24] Hossain A., Atique Ullah A.K.M., Guin P.S., Roy S. An overview of $\text{La}_2\text{NiMnO}_6$ double perovskites: synthesis, structure, properties, and applications. *J. of Sol-Gel Science and Technology*, 2020, **93** (3), P. 479–494.
- [25] Tauc J., Grigorovici R., Vancu A. Optical properties and electronic structure of amorphous germanium. *Phys. Status Solidi*, 1966, **15**, P. 627–637.
- [26] Park N.-G., Segawa H. Research direction toward theoretical efficiency in perovskite solar cells. *ACS Photonics*, 2018, **5** (8), P. 2970–2977.
- [27] Yang Z., Rajagopal A., Jen A.K.Y. Ideal bandgap organic–inorganic hybrid perovskite solar cells. *Adv. Mater.*, 2017, **29** (47), 1704418.

Submitted 18 May 2022; accepted 26 May 2022

Information about the authors:

Sergey S. Kozlov – Solar Photovoltaic Laboratory, Emanuel Institute of Biochemical Physics, Russian Academy of Sciences, Kosygin St., 4, Moscow, 119334, Russia; sergeykozlov1@gmail.com

Olga V. Alexeeva – Solar Photovoltaic Laboratory, Emanuel Institute of Biochemical Physics, Russian Academy of Sciences, Kosygin St., 4, Moscow, 119334, Russia; ORCID 0000-0001-8982-3959; alexol@yandex.ru

Anna B. Nikolskaia – Solar Photovoltaic Laboratory, Emanuel Institute of Biochemical Physics, Russian Academy of Sciences, Kosygin St., 4, Moscow, 119334, Russia; anickolskaya@mail.ru

Oleg I. Shevaleevskiy – Solar Photovoltaic Laboratory, Emanuel Institute of Biochemical Physics, Russian Academy of Sciences, Kosygin St., 4, Moscow, 119334, Russia; ORCID 0000-0002-8593-3023; shevale2006@yahoo.com

Denis D. Averkiev – St. Petersburg State Electrotechnical University “LETI”, Professora Popova St., 5, St. Petersburg, 197376, Russia; swnesli2019@gmail.com

Polina V. Kozhuhovskaya – St. Petersburg State Electrotechnical University “LETI”, Professora Popova St., 5, St. Petersburg, 197376, Russia; Ioffe Physical-Technical Institute, Russian Academy of Sciences, Politekhnikeskaya St., 26, St. Petersburg, 194021, Russia; polina219017@gmail.com

Oksana V. Almjashaeva – St. Petersburg State Electrotechnical University “LETI”, Professora Popova St., 5, St. Petersburg, 197376, Russia; Ioffe Physical-Technical Institute, Russian Academy of Sciences, Politekhnikeskaya St., 26, St. Petersburg, 194021, Russia; ORCID 0000-0002-6132-4178; almjasheva@mail.ru

Liudmila L. Larina – Solar Photovoltaic Laboratory, Emanuel Institute of Biochemical Physics, Russian Academy of Sciences, Kosygin St., 4, Moscow, 119334, Russia; llarina@yahoo.com

Conflict of interest: the authors declare no conflict of interest.